Full title: Hippocampal Dipeptidyl Peptidase 9 Bilaterally Modulates Memory via its Enzymatic Activity

Ya-Bo Zhao[1]† #, Shi-Zhe Wang[1, 2]†, Wen-Ting Guo[1, 2]†, Le Wang[1, 2], Lin Xu[1, 2], Qi-Xin Zhou[1, 2]*

1. Key Laboratory of Animal Models and Human Disease Mechanisms, and Laboratory of Learning and Memory, KIZ-SU Joint Laboratory of Animal Model and Drug Development, and State Key Laboratory of Genetic Resources and Evolution, Kunming Institute of Zoology, the Chinese Academy of Sciences (CAS), Kunming 650223, China.

2. University of Chinese Academy of Sciences, Beijing, 101408, China

*Corresponding authors: Q.X. Zhou (qixin_zhou@vip.126.com)

†These authors contributed to this work equally.

Present address: Y. B. Zhao, Technion - Israel Institute of Technology, Technion City, Haifa 3200003, Israel.

Keywords: DPP9, Learning, memory, Hippocampus, Proteomics

Highlights:

1. DPP9 is widely distributed throughout the whole brain, especially in the hippocampus.
2. DPP9 is necessary and sufficient for memory maintenance.
3. The enzymatic activity of DPP9 affects memory.
4. Proteins interacting with DPP9 are highly involved in learning and memory

Abstract

Dipeptidyl peptidase 9 (DPP9) has been extensively studied for its role in inflammation and cancer. DPP9-interacting proteins and substrates are involved in brain functions such as neuroinflammation, learning and memory, and anxiety. However, the function of DPP9 in the central nervous system remains unknown. Here, we found that DPP9 is highly expressed in hippocampal neurons and plays a crucial role in long-term potentiation and memory by electrophysiological and behavioral experiments and immunofluorescence staining. Proteomics analysis identified differentially expressed proteins associated with memory retrieval regulated by DPP9. Further investigation revealed that DPP9 enzymatic activity is essential for memory consolidation. DPP9-interacting proteins are involved in dendritic spine and axon function, and two memory- and axon-related genes, Tmp3 and Baiap2, were identified as potential targets for DPP9. Our findings suggest that DPP9 is a novel memory regulatory protein and provide new insights into memory molecular mechanisms.

Introduction

Dipeptidyl peptidase 9 (DPP9) is a member of the S9b serine protease family with post-proline dipeptidyl aminopeptidase activity, which cleaves Xaa-Pro dipeptides from the N-termini of proteins [1]. DPP9 is expressed in various tissues, including immune cells, liver, kidney, and brain[2-4]. It plays a biological role by cleaving specific substrates, such as Neuropeptide Y (NPY), peptide YY (PYY), and glucagon-like peptide-1 (GLP1) [5]. Recent studies have shown that DPP9 is involved in cancer, inflammation, and immune diseases [4, 6-8]. Inhibition of DPP9 activity has been demonstrated to reduce tumor growth and metastasis in animal models of cancer [9, 10]. In addition, inhibition of DPP9 has been shown to decrease T-cell proliferation and

cytokine production in animal models of autoimmune diseases [11-13]. Several studies have demonstrated that DPP9 can regulate the NLRP1 inflammasome to affect inflammation [14-16]. However, little is known about the role of DPP9 in the central nervous system.

The hippocampus is a vital brain region located in the medial temporal lobe and is responsible for learning and memory. It plays a crucial role in the formation and retrieval of declarative memories, such as facts, events, and personal experiences [17]. Memory is a complex process that involves the encoding, storage, and retrieval of information. However, the molecular mechanisms underlying memory are not yet fully understood [18, 19]. One of the critical processes involved in memory formation is synaptic plasticity, where synapses can strengthen or weaken in response to neural activity [20]. Long-term potentiation (LTP) is a form of synaptic plasticity. Specifically, the long-lasting enhancement of signaling between two neurons following synchronized stimulation. LTP is primarily observed in the hippocampus, a brain region critical for learning and memory. [21]. LTP is crucial in strengthening synaptic connections that underlie long-term memories.

In this study, we investigated the distribution of DPP9 in different brain regions and found that its expression in the dorsal hippocampus specifically affects memory in mice. This study demonstrates that DPP9 regulates several synaptic and memory-related proteins and that its enzymatic activity affects memory. Moreover, we found that DPP9 interacts with NPY in neurons and with the actin regulatory protein. These findings suggest that DPP9 plays a critical role in memory. Its interaction with NPY and other proteins may provide insight into the molecular mechanisms underlying memory formation and retrieval.

Result

DPP9 is widely distributed in neurons in different brain regions

There has been no previous study on the distribution of DPP9 protein in the brain. To investigate the distribution of DPP9 protein in the brain, we performed immunofluorescence staining of DPP9 and NeuN on distorted sections of the mouse brain (Fig 1. a). DPP9 expression was higher in the hippocampus, cerebellum, cortex, and olfactory bulb (Fig 1.b, and also supplement Fig 1. c-e). We measured DPP9 enzymatic activity in different brain regions and found that the hippocampus and olfactory bulb had the highest enzymatic activity, while the enzymatic activity of DPP9 in the thalamus and hypothalamus was relatively low (Fig 1. C). DPP9+ cells are

highly co-localized with NeuN+ cells in the hippocampus. Almost all hippocampal neurons express DPP9. (Fig 1.d, n=3, F (3, 16)=7.238, HIP vs. CBM *** $p<0.001$, HIP vs. OB *** $p<0.001$, Two-Way ANVOA). DPP9 also displayed some non-cell-specific signals on the slices, suggesting that it is secreted in the central nervous system. As a post-proline cleaving serine protease enzyme, it is a key indicator of DPP9 function[22]. This suggests that DPP9 may be involved in neuronal activities, particularly in the regulation of learning and memory, consistent with the high expression of DPP9 in the hippocampus observed in the Allen brain (supplement Fig 1 a, b)

Construction of the DPP9 overexpression and knockout mouse model

Based on the results obtained, we designed a CasRx-based DPP9 knockdown (KD) vector and a DPP9 overexpression (OE) vector and generated two adeno-associated viruses (AAVs) (Fig 2. a, d). We first verified the efficiency of the knockdown sgRNAs in cells (supplement Fig 2 a-d). Subsequently, we injected DPP9 KD AAV along with GFP AAV into the dorsal hippocampus of mice to ensure the accuracy of the injection position. After 21 days of expression, perfusion samples were collected for immunofluorescence staining, and western blot analysis was performed to confirm the knockdown efficiency (Fig 2. b). The results showed a significant decrease in DPP9 expression in the dorsal hippocampus (Fig 2. c, n=3, *$p=0.010$, t- test). Similarly, we injected DPP9 OE AAV into the dorsal hippocampus of mice and observed a significant increase in DPP9 expression after 21 days (Fig 2. e, f, n=3, **$p=0.002$, t- test) (western blot raw file in supplement Fig 6). Since exogenously expressed DPP9 carried the FLAG tag, we used FLAG staining to distinguish endogenous DPP9. In summary, we successfully established DPP9 knockdown and overexpression models using AAV-mediated gene delivery

DPP9 affects long-term memory maintenance but not acquisition process

Since the hippocampus is critical for learning and memory and DPP9 is highly expressed in the hippocampus, we investigated the role of DPP9 in these processes. To reduce animal use, we conducted a series of behavioral tests on the same mice. Tests were separated by at least 24 hours to minimize interference and to start with tests that had weaker stimulation. We used open-field experiments to examine whether DPP9 affects mice's spontaneous behavior and locomotion. We

found that DPP9 KD and OE mice did not exhibit changes in movement speed or distance (supplement Fig 3. a, n=12, p=0.892, b, n=12, p=0.780, c, n=8, p=0.183, d, n=8, p=0.839 t- test). We then conducted novel object recognition experiments to test long-term memory and found that DPP9 KD mice exhibited significant impairment in their ability to distinguish new and old objects after 24 hours (supplement Fig 3. g, n=11, **p=0.003, t- test), while DPP9 OE mice sniffed new objects significantly longer than the control group (supplement Fig 3. h, n=9, **p=0.003, t- test). Next, we conducted an elevated plus maze experiment to detect anxiety behavior in mice, and the results showed that DPP9 OE and DPP9 KD did not affect the time mice spent in the open arm (supplement Fig 3. e, n=12, p=0.263, f, n=11, p=0.971, t test). Finally, we used a conditioned fear test to simultaneously examine learning and long-term memory in mice, specifically the contextual fear conditioning test. Since memory is enhanced after DPP9 OE, we designed different foot shock modes for DPP9 OE and KD. We used weaker foot shocks (0.5 mA, 3 times) to detect memory enhancement after DPP9 OE((Fig 2. g) and stronger foot shocks (0.8 mA, 6 times) to detect memory impairment after DPP9 KD((Fig 2. h). Notably, neither KD nor OE of DPP9 affected the learning performance of mice (Fig 2. i, n=8, F(1, 14)=0.079, p=0.781, k, n=10, F(1, 19)=0.286, p=0.598, two-way ANOVA). The results of memory retrieval 48 hours after learning were consistent with the novel object recognition experiment, and the freezing behavior of DPP9 KD mice was significantly reduced (Fig 2. j, n=7, **p=0.003, l, n=9, **p=0.007, t test); the freezing behavior of DPP9 OE mice was significantly increased. In conclusion, our results show that KD or OE of DPP9 in the dorsal hippocampus does not affect the spontaneous movement, anxiety behavior and learning of mice but strongly affects the memory of mice.

DPP9 regulates memory by enzymatic activity

We demonstrated that DPP9 plays a significant role in memory, but the mechanism by which DPP9 affects memory is still unclear. We investigated the role of DPP9 in memory and identified differentially expressed proteins (DEPs) using proteomics. We performed extraction 48 hours after the strong learning model (CFC, 0.8 mA, 6 times) and removed the hippocampal tissue for enzymatic digestion after 4 hours of extraction, with data-independent acquisition (DIA) and DIA-NN analysis (Fig 3. a). Principal component analysis (PCA) results showed that the principal components of DPP9 knockdown (KD) and overexpression (OE) partially overlapped with their

respective controls, but most of them were separated, indicating that changes in the expression of DPP9 affect many proteins in the hippocampus (Fig 3. b, c). Subsequent volcano plot analysis also confirmed the PCA results. We found 539 DEPs with P value <0.05 in the DPP9 knockdown protein group (Fig 3. d, including 57 DEPs with log (Fold Change) <0.5, log (Fold Change)>0.5 DEPs 154); the DPP9 overexpressed protein group contained 1354 DEPs with P value < 0.05 (Fig 3. e, 240 DEPs with log (Fold Change) <0.5, 456 DEPs with log (Fold Change)>0.5). At the same time, we used the top 100 proteins with the smallest P value to draw a hierarchical clustering heatmap and KEGG and GO pathway enrichment (supplement Fig 2).

Then, we used GSEA to identify the signaling pathways in which DPP9 OE and KD participated in the opposite trend. The endopeptidase regulation activity pathway was enriched (Fig 3. f), and we also enriched serine endopeptidase inhibitor activity (Fig 3. g), which indicated that DPP9 exhibited the characteristics of serine proteases in the hippocampus. After that, we found that a peptide related to learning and memory, neuropeptide Y (NPY), is the substrate of DPP9, so we designed a series of experiments to prove the relationship between NPY and DPP9 in the hippocampus[23]. First, we examined the colocalization of DPP9 and NPY and observed that DPP9 was co-expressed in NPY+ neurons in the hippocampus (Fig 3. h). However, this does not prove that DPP9 interacts with NPY in the hippocampus because NPY is the substrate of DPP9, and it is not feasible to detect it using traditional protein interaction methods (such as CO-IP). We used a proximity ligation assay (PLA) to detect the interaction between DPP9 and NPY in situ in the hippocampus, and the results showed that this interaction existed in the hippocampus (Fig 3. i).

To further explore the effect of DPP9 and DPP9 enzymatic activity on memory, we first tested hippocampal LTP in DPP9 KD and OE mice. Long-term potentiation (LTP) is an important cellular mechanism for memory storage in the hippocampus and is also one of the important manifestations of synaptic plasticity [24]. We performed LTP tests using hippocampal slices of mice injected with DPP9 KD or OE AAV for 21 days. Using three trains of 100 Hz high-frequency stimulation (HFS) to induce LTP in hippocampal slices of DPP9 knockdown and control mice, we found that LTP was significantly attenuated after DPP9 KD (Fig 3. j, k, l, n=7, **p=0.003, t test). In contrast, LTP was significantly enhanced after DPP9 OE when HFS induced LTP in hippocampal slices of DPP9 OE and control mice (Fig. 3m, n=7, ***p<0.001, t test). After that, we utilized Val-boroPro (VBP) to test DPP9 enzymatic activity on LTP. VBP is a nonselective

inhibitor of post-proline cleaving serine proteases. It can inhibit DPP4, DPP8, and DPP9 [25]. When 10 μM VBP was used, the LTP induced by HFS was significantly weakened (supplement S3), and 20 μM VBP completely blocked LTP. Although some studies have shown that DPP4 is not expressed in neurons (Fig 3. o, p, n=6, **p=0.002, t test), we used the DPP4-specific inhibitor sitagliptin to rule out the role of DPP4. We observed no change in HFS-induced LTP after high doses (50 μM) of sitagliptin were administered (Fig 3. q, r, n=6, p=0.684, t test).

Finally, we implanted the cannula in the hippocampus of the mice, performed memory retrieval 48 hours after experiencing 6 foot shocks, and injected 1 μL of 500 μM VBP 10 minutes before the extraction. We found that the freezing behavior of mice was significantly reduced when an audio stimulus was given (supplement S3). The above experimental results proved that DPP9 is involved in the NPY condition, and the enzyme activity and expression of DPP9 can affect the memory and synaptic plasticity of mice.

DPP9-interacting proteins are involved in memory processes

To investigate the potential binding of DPP9 to other proteins in the hippocampus and its impact on memory, we conducted coimmunoprecipitation (CO-IP) and proteomics experiments to identify the proteins that interact with DPP9 in this region. Specifically, we expressed FLAG-tagged DPP9 (DPP9-FLAG) in the hippocampus, used magnetic beads with FLAG antibody to pull down DPP9-FLAG, digested the protein, and identified its interacting partners using mass spectrometry (Fig 4. a). We analyzed four samples and selected proteins that were detected in at least two samples simultaneously. In total, we identified 77 proteins that interact with DPP9. To gain further insight into the functions of these proteins, we performed string protein network interaction analysis (PPI) and used betweenness analysis and sorting. We placed proteins with higher interactions in the inner circle and marked them in pink, while those with lower interactions were placed outside the circles and marked in green (Fig 4. b). We also conducted GO enrichment analysis on the 77 proteins and found that they were highly associated with protein polymerization and actin functions (Fig 4. c). Notably, actin functions are closely linked to synaptic plasticity and memory [26].

Next, we used a Venn diagram to identify the differentially expressed proteins (DEPs) in both DPP9 knockdown (KD) and overexpression (OE) cells and found 163 DEPs common to both

groups (Fig 4. d). We combined these essential DEPs with the proteins discovered by co-IP and identified two key proteins, Tpm3 and Baiap2 (Fig 4. e). We demonstrated that DPP9 regulates the expression of these two proteins, with Tpm3 significantly decreased in DPP9 KD and significantly increased in DPP9 OE cells (Fig 4. f, n=5, **p=0.004, g, n=5, *p=0.04, t test). Since Tpm3 regulates axon structure, we analyzed axon guidance-associated DEPs (Fig 4. h). In contrast, Baiap2 was downregulated in both DPP9 KD and OE cells but more significantly downregulated in DPP9 OE cells (Fig 4. i, n=5, *p=0.046, j, n=5, ***p<0.001, t test). As Baiap2 is involved in the regulation of postsynaptic functions, we concluded that DPP9 affects postsynaptic functions (Fig 4. k).

We performed KEGG pathway and GO enrichment analyses on these DEPs and found that they were highly enriched in neural and synapse-related pathways (Fig 4. l, m). Notably, immune-related pathways were enriched in GSEA, indicating that DPP9 may also regulate proteins related to neuroimmune functions (supplement S2, f, g). Our findings provide a theoretical basis for how DPP9 affects memory by regulating the proteins that interact with it, particularly those involved in neuronal and synaptic functions. Finally, we identified two key proteins Tpm3 and Baiap2 that interact with and are regulated by DPP9, further supporting our hypothesis that DPP9 plays a role in memory.

Discussion

Previous studies on DPP9 have mainly focused on cancer and immune diseases, but we revealed the role and mechanism of DPP9 in memory. Using immunofluorescence staining of DPP9 and NeuN, we observed that DPP9 is widely expressed in the brain and is likely present in most neurons. These results were confirmed by FISH analysis in the Allen Brain. Interestingly, DPP9 was also found to be expressed in nonneuronal cells in the cerebellum and olfactory bulb, suggesting its involvement in significant functions in these brain regions. In addition, our immunofluorescence staining indicated that DPP9 had a strong signal in noncellular areas. After excluding the cause of nonspecific staining, we hypothesized that DPP9 may be a secreted protein in the central nervous system. Although it is commonly believed that DPP9 lacks transmembrane regions and secretion signals and exists in the cytoplasm, some studies have reported the presence of soluble DPP9 in serum[1, 27-29]. Due to the neonatal lethality of DPP9, we were unable to

establish an effective knockout mouse strain. Therefore, we used an AAV vector to knock down the target brain region in a more convenient and efficient manner. [30, 31]. CasRx is a knockdown solution discovered in recent years. It requires a more specific gRNA, and unlike RNAi, which relies on its own RNA-induced silencing complex, it has lower off-target efficiency and higher knockdown efficiency [32-34].

The hippocampus is generally divided into the dorsal and ventral halves. The dorsal side is more involved in learning and memory, while the ventral side is more involved in emotion and emotion regulation. [35]. We modulated DPP9 in the dorsal hippocampus and found that DPP9 did not affect spontaneous and anxious behavior in mice. This is consistent with previous reports on the dorsal hippocampus [36, 37]. The strong effect of DPP9 on memory and synaptic viability suggests that it is critical to memory-related behaviors. It is worth noting that the change in DPP9 does not affect the learning of mice. This is combined with DPP9 affecting the maintenance of LTP. This indicates that DPP9 regulates the maintenance and extraction of memory and does not participate in the acquisition of acquired information.

When we used proteomics to study the mechanism by which DPP9 might be involved in memory, we found that DPP9-derived DEPs were highly involved in synaptic function and memory-related pathways, which validated our behavioral and electrophysiological results as a whole. At the same time, we also found that there were many differences between the DEPs of DPP9 KD and DPP9 OE. First, this may be because the effect of OE is better than that of KD. More importantly, we analyzed the DEPs of DPP9 KD and DPP9 OE to enrich the pathway separately. These pathways suggest that DPP9 OE more directly regulates glutamate receptors and synaptic structures. This to some extent indicates that more or less DPP9 expression may be involved in different neuron functions. Subsequently, we found that DPP9 played the role of peptidase in the hippocampus. Although NPY was proven to be the substrate of DPP9 in previous studies, it was not clear whether DPP9 was involved in the regulation of NPY in vivo[38, 39]. Our study demonstrates that DPP9 has a direct interaction with NPY in the hippocampus, and inhibition of enzyme activity can impair LTP and memory in mice. NPY is cleaved from full-length NPY 1-36 to NPY 3-36 by DPP9, and these two NPYs play different roles in the nervous system. NPY 1-36 mainly binds to the Y1 Y2 Y5 receptor, while NPY3-36 only binds to the Y2 Y5 receptor. Some studies have shown that activation of the Y1 receptor and injection of NPY can

reduce fear memory in rats, while Y2 agonists have no such effect[23, 40, 41]. At the same time, NPY also impairs the maintenance of LTP, which is also consistent with our findings [42]. Our study suggests that DPP9 may regulate the ratio of NPY1-36 to NPY3-36 to affect learning and memory.

In addition to participating in biological functions through enzymatic activity, DPP9 also participates in protein interactions [16, 43, 44]. We found that DPP9 interacts with learning- and memory-related proteins Ppp1r9b, Rac1, Ppp2r1a, etc. Rac1 strongly affects memory and forgetting [45, 46]. Many studies have shown that actin is an important protein that maintains the morphology and occurrence of dendritic spines, and affecting the aggregation of actin can regulate learning and memory [26, 47-49]. We found that DPP9-interacting proteins are highly involved in the aggregation of actions and localized in the spine, which indicates that DPP9 is likely to be directly involved in the maintenance of direct synaptic connections. Meanwhile, we found two key proteins regulated by DPP9, Tpm3 and Baiap2. Tpm3 is a kind of tropomyosin that is an important protein that regulates actin. It is enriched in the postsynaptic region. Its deletion destroys the function of the axon initial segment and reduces the firing frequency [50, 51]. Baiap2 is the abbreviation of BAR/IMD Domain Containing Adapter Protein 2 and exists in postsynaptic density [52]. Research reports that Baiap2 is related to various psychiatric diseases and participates in the regulation of memory [53-55]. A study suggests that mutations in Baiap2 lead to severe learning deficits [56]. This evidence shows that DPP9 can affect memory simultaneously from the two aspects of enzyme activity and protein interaction.

In a proteomic study on memantine improving the cognition of Triple Transgenic Mouse of Alzheimer's Disease (AD), DPP was found to be the most downregulated protein [57]. Another recent study showed that the downregulation of DPP4 contributes to the improvement of AD symptoms, which is mainly due to the involvement of DPP4 in the cleavage of pyroGlu3–Aβ. [58]. Although DPP4 is hardly expressed in the brain, the use of DPP4 inhibitors in APP/PS1 mice can also improve AD symptoms. This is likely to be related to changes in the permeability of cerebral blood vessels in AD [59]. In the brain, DPP9 and DPP4 show similar enzymatic activity. DPP9 is likely to play a more important role in the treatment of AD. At the same time, some studies have also confirmed that Aβ activates the NLRP1 inflammasome, thereby triggering severe neuroinflammation and neurotoxicity [14, 60, 61]. DPP9 can inhibit NLRP1 through enzymatic

activity and FIIND domain binding[15]. Based on these studies, we found that DPP9 seems to play an important role in the treatment of AD, which will also be our future research direction.

There are also many deficiencies in this study. First, we did not construct a conditional KO mouse, which led to our inability to completely knock out the expression of DPP9 in the hippocampus. Although CasRx obtained better knockdown results, our proteome results showed that the knockdown DEPs were significantly fewer than OE. Second, we did not study the effect of DPP9 on short-term memory. STM and LTM have different mechanisms, and DPP9 may have different regulatory effects on STM[62] Finally, we did not conduct further research on the two key proteins found, Tpm3 and Baiap2. However, we plan to conduct more detailed research on these two proteins and DPP9 in the future.

In summary, we systematically studied the distribution of DPP9 in the central nervous system and its role and mechanism in memory. We found that DPP9 is widely distributed in the brain, especially in the hippocampus, with high expression. Then, we found that interfering with the expression of DPP9 in the dorsal hippocampus of mice can specifically regulate memory in mice. We used proteomics technology to detect the pathways regulated by DPP9 and concluded that DPP9 affects memory through enzyme activity. Finally, we used co-IP technology to discover proteins interacting with DPP9 and suggested that DPP9 is involved in the regulation of actin aggregation. Therefore, we found that DPP9 has a crucial function in the central nervous system. This function has never been reported before, which provides novel evidence for revealing the mechanism of memory.

Acknowledgments

We would like to thank the Institutional Center for Shared Technologies and Facilities of Kunming Institute of Zoology (KIZ), Chinese Academy of Sciences (CAS) for providing us with mass spectrometry. And we are grateful to Lin Zeng for technical support. We are also grateful to Yu Pan from Technion - Israel Institute of Technology who helped us discuss and draw illustrations.

Contribution

Conceptualization: Y.B.Z and Q.X.Z; Methodology: Y.B.Z; Formal Analysis: Y.B.Z; Investigation:

Y.B.Z, S.Z.W, LW; Writing – Original Draft: Y.B.Z; Writing – Review & Editing: Y.B.Z, Q.X.Z and W.T.G; Visualization: Y.B.Z; Supervision: Q.X.Z, L.X and Y.B.Z; Funding Acquisition: L.X and Q.X.Z

STAR Methods

REAGENT or RESOURCE	SOURCE	IDENTIFIER
Antibodies		
Rabbit Polyclonal anti-DPP9	Abcam	ab42080
Mouse Monoclonal anti-NeuN	Millipore	ABN78B
Mouse Monoclonal anti-NPY	Santa Cruz	sc-133080
Rabbit Monoclonal anti-DPP9	Origene	TA503937
Mouse Monoclonal anti-FLAG	Sigma aldrich	F3165
Anti-mouse H+L HRP-conjugated IgG	Proteintech	SA00001-1
Donkey anti-rabbit H+L Alexa Fluor Plus 488	Invitrogen	A32790
Goat anti-mouse H+L Alexa Fluor Plus 555	Invitrogen	A32727
Bacterial and virus strains		
AAV2/9-CMV-Cax13d-FLAG-U6-2x gRNA(DPP9)	Shandong Vigene Biosciences Co., Ltd	N/A
AAV2/9-hSyn-GFP-WPRA	Shandong Vigene Biosciences Co., Ltd	N/A
AAV2/9-CMV-Cax13d-FLAG-U6-2x gRNA (random)	Shandong Vigene Biosciences Co., Ltd	N/A
AAV2/9-hSyn-DPP9-FLAG- WPRA	Shandong Vigene Biosciences Co., Ltd	N/A
Chemicals, peptides, and recombinant proteins		
Zoletil 50	Virbac Animal Health India Pvt Ltd	N/A
Xylazine	Shanghai Aladdin Biochemical Technology Co., Ltd.	X113956
Ibuprofen	Shanghai Aladdin Biochemical Technology Co., Ltd.	I129291
DTT	Shanghai Aladdin Biochemical Technology Co., Ltd.	D104860
Iodoacetamide	Shanghai Aladdin Biochemical Technology Co., Ltd.	I131590
Val-boroPro	MedChemExpress	HY-13233A
Sitagliptin	MedChemExpress	HY-13749B
Citrate buffer solution	Beyotime	P0081
Donkey serum	Solarbio	SL050
Goat serum	Solarbio	SL038
DAPI	Beyotime	C1005
ProLong Glass Antifade Mountant	Invitrogen	P36980
Protease inhibitors	Thermo	87785
QuickBlock Blocking Buffer	Beyotime	P0220
Lys-C	Wako	125-05061
Trypsin	Promega	V5280

3XFLAG peptide	MedChemExpress	HY-P0319A
Critical commercial assays		
Pierce Rapid Gold BCA kit	Thermo	A53225
DPPIV-Glo Protease Assay Kit	Promega	G8350
Duolink In Situ Detection Reagents Orange	Sigma aldrich	DUO92007
Protein G magnetic beads	Invitrogen	10004D
NUPAGE gels	Invitrogen	NP0322
Silver staining Kit	Beyotime	P0017S
Deposited data		
Proteomic data	This paper	PXD044715
Experimental models: Organisms/strains		
C57BL/6J	SPF (Beijing) biotechnology co., LTD	N/A
Software and algorithms		
DIA-NN 1.8.1	Demichev, V., et al.	https://github.com/vdemichev/DiaNN
Proteome Discoverer 2.4	Thermo	https://www.thermofisher.com/
FIJI	NIH	https://mirror.imagej.net/
Quantity One	Bio-rad	https://www.bio-rad.com/
pCLAMP 10	Molecular devices	https://www.moleculardevices.com/
Activity Monitor	Med Associates Inc	https://med-associates.com/
VideoFreeze™ Video Fear Conditioning Software	Med Associates Inc	https://med-associates.com/
GraphPad Prism 9.2.0	GraphPad Software Inc	https://www.graphpad.com/scientific-software/prism/
cellSens	Olympus	https://www.olympus-lifescience.com/
R Studio	CRAN R Project	https://cran.r-project.org/
STRING	Szklarczyk et al., 2019[63]	https://string-db.org/
Cytoscape 3.10	Shannon et al., 2003[64]	https://cytoscape.org/
Other		
30K ultrafiltration tube	Pall Life Sciences	OD010C34
C18 25 cm × 75 μm column	Thermo	164941
SDB-RPS	Empore	2241
Nanoliter-volume injection pump	WPI	Micro4
Laser confocal microscope	Olympus	FV3000
Chemiluminescence detection system	Tanon	5200
Microplate reader	Allsheng	A300
Vibratome	Leica	VT1000s
Amplifier	Molecular Devices	Multiclamp 700B
Digitization	Molecular Devices	Digidata 1440A
Open field device	Med Associates Inc.	MED-OFAS-MSU
Elevated Plus Maze	Med Associates Inc.	ENV-560A
Fear Conditioning System	Med Associates Inc.	MED-VFC2-USB-M

LC–MS	Thermo	UltiMate 3000 Q Exactive
LC–MS	Thermo	EASY-nLC 1000 Orbitrap Fusion Lumos

319

Animal

Adult male C57BL/6J mice (from the SPF (Beijing) biotechnology co., LTD, 6-8 weeks of age, weighing 18–22 g) were used. At the Kunming Institute of Zoology, animals were housed in cages with four animals each and provided with free access to food and water under a 12-hour light/dark cycle in a temperature-regulated environment. Tunnel handling was performed every day for 4 days before the behavioral experiment, and the tunnel was used when the mice were transferred in the behavioral experiment[65]. The experimental procedures were approved by the Animal Ethics Committee of the Kunming Institute of Zoology (No. IACUC-RE-2021-06-012).

Stereotaxic injection

Mice were anesthetized with Zoletil 50 (40 mg/kg) and xylazine (10 mg/kg), haired by clipper, and fixed in a stereotaxic instrument (RWD, China). Remove the soft tissue from the skull after cutting the scalp. Microdrilling holes in the skull after leveling the skull. The coordinates of the hippocampus were 1.7 mm along the AP axis, ±1.5 mm on the medial-dorsal (ML) axis, and 1.8 mm dorsal-ventral (DV) depth with respect to bregma. A nanoliter-volume injection pump (Micro4, WPI, USA) was used to inject 500 nl of virus (injection speed of 50 nl/min) into each hippocampus. After the injection, leave the glass pipette for 5 minutes and pull it out. Finally, the mouse's scalp was sutured and put back into the home cage. Ibuprofen (10 mg/kg) was given for pain relief within 3 days after the operation.

DPP9 Knockout and overexpression

Knockout and overexpression were performed using AVV vectors (Shandong Vigene Biosciences Co., Ltd). The DPP9 KD group was injected with AAV2/9-CMV-Cax13d-FLAG-U6-2x gRNA(DPP9) mixed with AAV2/9-hSyn-GFP-WPRA. The gRNA sequences of DPP9 were 3'CCCCATAGACAAAGAGCACAGTG5' and 3'AGTCTCGATGTTTGCCCACCCACA5'; the DPP9 KD control group was injected with AAV2/9-CMV-Cax13d-FLAG-U6-2x gRNA (random) mixed with AAV2/9-hSyn-GFP-WPRA. The DPP9 OE group was injected with AAV2/9-hSyn-DPP9-FLAG mixed with AAV2/9-hSyn-GFP-WPRA; the DPP9 OE control group was only injected with AAV2/9-hSyn-GFP-WPRA.

Immunofluorescence staining

Mice were perfused with 50 ml phosphate-buffered saline (PBS) after anesthesia, followed by 150 ml of 4% PFA. The brains were kept in 4% PFA at 4°C overnight and dehydrated twice using 30% sucrose. The brains were frozen after being embedded in OCT compound. For immunofluorescence staining, 15 μm slices were washed 3 times with PBS containing 0.3% Triton X100 (PBST). The slices were placed into citrate buffer solution (Beyotime, P0081) for antigen retrieval (microwave oven, low power, 20 min). Sections were blocked with 1.5% donkey and goat serum (Solarbio, SL050, SL038) in PBST (blocking buffer) after returning to room temperature for 1.5 h. Slides were incubated with primary antibodies (rabbit anti-DPP9, Abcam, ab42080, 1:250; mouse anti-NeuN, Millipore ABN78B, 1:500; mouse anti-NPY, Santa Cruz, sc-133080, 1:500) diluted in blocking buffer for 24 h at 4°C. After incubation, the cells were washed with PBST 3 times. The secondary antibody (donkey anti-rabbit Alexa Fluor Plus 488, Invitrogen, A32790, 1:1000; goat anti-mouse Alexa Fluor Plus 555, Invitrogen, A32727, 1:1000) was diluted with blocking buffer, and the slices were incubated at room temperature for 1 h. After washing 3 times with PBST, the slides were incubated with DAPI (Beyotime, C1005) and then mounted with ProLong Glass Antifade Mountant (Invitrogen, P36980). After the mounting medium was dried for 10 h, it was photographed with an FV3000 laser confocal microscope (Evident, Japan).

Western blotting

The mouse brain was quickly removed 21 days after viral injection, and hippocampal tissues were placed in ice-cold PBS. The tissue was homogenized in RIPA buffer and protease inhibitors (Thermo, 87785) for 1 min on ice and then centrifuged at 10,000 x g for 10 min at 4°C. The supernatants of the samples were assayed for protein content using a Pierce Rapid Gold BCA kit (Thermo, A53225), diluted with LDS sample buffer (Invitrogen, NP0007) and 50 mM DTT and then heated at 70°C for 10 min. The proteins were loaded onto 10% PAGE gels and transferred onto PVDF membranes. The membranes were blocked with QuickBlock Blocking Buffer (Beyotime, P0220). The membranes were incubated with the following primary antibodies overnight at 4°C: mouse anti-DPP9 (Origene, TA503937, 1:1000). After three washes with TBST, the membranes were incubated with anti-mouse H+L HRP-conjugated IgG (Proteintech, SA00001-1, 1:10000) for 1 h at room temperature, washed with PBS, and scanned with a

chemiluminescence detection system (Tanon, China).

DPP8/9 enzyme activity

The DPPIV-Glo Protease Assay Kit (Promega, G8350) was used for DPP9 enzyme activity analysis. Briefly, the hippocampus was homogenized in TE buffer (pH 8.0) with 10 μM sitagliptin and centrifuged at 10,000 x g for 10 min at 4°C[66]. The supernatant was diluted 50 times. The substrate and buffer were mixed to prepare the reaction buffer. The diluted supernatant and reaction buffer were mixed in a 96-well plate and incubated at 37°C for 20 min. A microplate reader (Allsheng, China) was used to detect the intensity of chemiluminescence.

Proximity Ligation Assay (PLA)

Following the protocol of Duolink In Situ Detection Reagents Orange (Sigma, DUO92007), PLA experiments were conducted. Briefly, sections were blocked with donkey and goat serum after permeabilization and antigen retrieval. Primary antibodies (rabbit anti-DPP9, Abcam, ab42080, 1:250; mouse anti-NPY, Santa Cruz, sc-133080, 1:500) were added to the blocking buffer and incubated overnight at 4°C. After washing with PBST 3 times, anti-mouse (MINUS) and anti-rabbit (PLUS) probes were added and incubated for 2 h at room temperature. The samples were washed 3 times and incubated with ligation and ligase at 37°C for 30 min. After washing, polymerase was incubated with amplification at 37°C for 100 min. The slides were incubated with DAPI (Beyotime, C1005) and then mounted with ProLong Glass Antifade Mountant (Invitrogen, P36980). After the mounting medium was dried for 10 h, it was photographed with an FV3000 laser confocal microscope (Evident, Japan).

Electrophysiological record

For LTP recordings of DPP9 KD and OE mice, brain slices (350 μm) were removed 21 days after the mice were injected with AAV. After mice were anesthetized with isoflurane, the brains were quickly removed and placed in ice-cold saturated carbogen (95% O2, 5% CO2) artificial cerebrospinal fluid (ACSF) (120 NaCl, 2.5 KCl, 26 NaHCO3, 1.25 NaH2PO4, 2 MgSO4, 10 D-glucose and 2 CaCl2, mM). After slicing with a vibratome (Leica, German), the brain slices were placed in ACSF with carbogen at 30°C for 30 min and then maintained at room temperature for at

least 1 hour. The brain slices were placed in the immersion chamber, and ACSF was continuously perfused with carbogen at a flow rate of 2-4 ml/min. The stimulating electrodes (made of a pair of wound Teflon-coated platinum-iridium alloys, WPI) were placed on Schaffer collaterals (SCs); the recording electrodes (made of borosilicate glass capillary drawn, 1 MΩ, PG10165, WPI) were placed in the stratum radiatum of the dorsal CA1 area of the hippocampus. Record for at least 20 min at 0.033 Hz to establish a stable baseline with a stimulus intensity set to elicit an equivalent maximum fEPSP slope of approximately 40-50%. LTP was then induced by high frequency stimulation (HFS, 3 columns of 1 s stimulation at 100 Hz with a 20 s interval between columns) at the same stimulus intensity as that used for baseline recordings. For recordings using inhibitors, brain slices were placed in ACSF with carbogen-containing inhibitors (Val-boroPro, MedChemExpress, HY-13233A; Sitagliptin, MedChemExpress, HY-13749B) 30 min before placement in the chamber, and the ACSF perfused in the chamber also contained inhibitors. Signals were acquired using a Multiclamp 700B and Digidata 1440A (Molecular Devices, USA) and digitized at a sampling rate of 20 kHz.

Novel object recognition test

This experiment was performed as previously described[67]. In short, the day before the NOR test, the mice were placed in an empty box (50 × 50 × 40 cm, white PMMA) to move freely for 10 minutes, allowing them to habituate to the context. Two identical objects (Lego blocks) were placed on both sides of the box 5 cm away from the wall, and the mice were placed into the box to move freely for 10 minutes. After 24 hours, the mouse was put back into the box after replacing the old object of the previous day with a new object (plaster cast). The time for the mice to explore the new object and the old object were recorded separately. After each mouse experiment, the box was thoroughly cleaned with 75% ethanol. The method to calculate the preference index is to subtract the old object exploration time from the new object exploration time and divide by the total exploration time (the new object exploration time plus the old object exploration time).

Open field test

The mice were placed in the open field device (Med Associates Inc., MED-OFAS-MSU) and moved freely for 15 minutes. After each mouse experiment, the box was thoroughly cleaned with

75% ethanol. Data were analyzed using Activity Monitor 7 Software.

Elevated Plus Maze

The mice were placed in the experimental room for at least 1 hour before the experiment. The mice were placed on the Elevated Plus Maze (Med Associates Inc., ENV-560A) and allowed to move freely for 5 min. After each mouse experiment, the box was thoroughly cleaned with 75% ethanol. A stopwatch was used to record the time the mice stayed in the open and closed arms.

Contextual fear conditioning

The day before the plantar electric shock, the mice were placed in the Fear Conditioning System (Med Associates Inc., MED-VFC2-USB-M) for 10 minutes to allow the mice to habituate to the context. The next day, the mice were placed in the fear conditioning system. For DPP9 OE mice, we administered 3 foot shocks (0.5 mA, two minutes apart); for DPP9 KD mice, we administered 5 foot shocks (0.8 mA, session of shock stimulus interval (s): 150, 90, 80, 100, 70). After the shock, the mice were returned to their home cages. After 48 hours, we placed the mice back into the fear conditioning system for 5 minutes to retrieve the memory.

Proteome sample preparation and LC□MS

Sample preparation was performed using filter-aided sample preparation (FASP)[68]. Briefly, the hippocampal tissue of the mice was removed 4 hours after the CFC experiment. The tissue was homogenized in lysis buffer (100 mM NaCl, 50 mM Tris, 0.5% Triton X-100, 0.5% SDS, pH 7.4) containing protease inhibitors (Thermo, 87785) for 1 min on ice and then centrifuged at 10,000 x g for 10 min at 4°C. The supernatants of the samples were assayed for protein content using a Pierce Rapid Gold BCA kit (Thermo, A53225). Fifty micrograms of protein was added to DTT (Aladdin, D104860) to a final concentration of 20 mM and heated at 90°C for 10 min to reduce the protein. Afterwards, iodoacetamide (Aladdin, I131590) at a final concentration of 40 mM was added for alkylation at 37°C in the dark for 30 min. Then, 5 times the volume of UA buffer (8 M urea, 100 mM Tris, pH 8.0) was added, and the mixture was placed into a 30K ultrafiltration tube (Pall Life Sciences, OD010C34) for cleaning (12000xg centrifugation for 15 min). The ultrafiltration tube was cleaned with UA buffer 3 times. Then, 0.5 μg Lys-C (Wako, 125-05061) was added and

incubated at 37°C for 4 hours. Then, 1 μg trypsin (Promega, V5280) was added and digested at 37°C for 8 hours. The samples were desalted with a homemade stage tip (ion exchange SDB-RPS, Empore, 2241) after enzymatic digestion[69]. Samples were dried using a Speedvac and reconstituted with 0.1% formic acid in water. The concentration of the peptide was measured using the absorbance at A280. The peptide solution (800 ng) was injected into an UltiMate 3000 RSLC nano System (Thermo, USA) with a C18 25 cm × 75 μm column (Thermo, 164941). The mass spectrometer was Q Exactive (Thermo, USA). The peptides were eluted with 2–28% buffer B (0.1% [vol/vol] formic acid, 80% acetonitrile) with a nonlinear 90 min gradient at a flow rate of 300 nL/min.

Samples were run on the Q Exactive mass spectrometer with a Data Independent Acquisition (DIA) method for peptide MS/MS analysis. Full scans of peptide precursors were performed from 350 to 1490 m/z at 70 K FWHM resolution with a 3×10^6 AGC target and a maximum IT of 100 ms. After a full scan, a variable window was used to acquire DIA from 150 m/z at 17.5 K FWHM resolution (at 200 m/z) with a 1×10^6 AGC target and a maximum IT of 100 ms. HCD fragmentation was applied with 26% collision energy. All data were searched using the spectral library free of DIA-NN 1.8.1 and the precursor FDR set at 1.0%[70].

Affinity purification mass spectrometry (AP-MS)

The hippocampus was removed 21 days after mice were injected with AVV of DPP9 OE. The tissue was homogenized in lysis buffer (100 mM NaCl, 50 mM Tris, 0.5% NP-40, 10% glycerin, pH 7.4) containing protease inhibitors (Thermo, 87785) for 1 min on ice and then centrifuged at 10,000 x g for 10 min at 4°C. Mouse anti-FLAG antibody (Sigma, F3165) and Protein G magnetic beads (10004D, Invitrogen) were added to the supernatant and incubated at 4°C for 3 hours. The magnetic beads were washed 4 times with PBST buffer. 3XFLAG peptide (MedChemExpress, HY-P0319A) was added for competitive elution. The eluate was added to LDS sample buffer (Invitrogen, NP0007) and 50 mM DTT and then heated at 70°C for 10 min. The proteins were loaded onto NUPAGE gels (Invitrogen, NP0322), and the gels were stained with silver staining (Beyotime, P0017S) after electrophoresis. The gel slices were excised for in-gel digestion[71]. Briefly, gel slices were reduced and alkylated with DTT and iodoacetamide after destaining. After adding 1 μg of trypsin overnight at 37°C, acetonitrile was added to extract the peptides. Use a

homemade STAGE tip to desalt. Samples were dried using a Speedvac and reconstituted with 0.1% formic acid in water. The peptide solution was injected into an EASY-nLC 1000 (Thermo, USA) with a homemade C18 20 cm × 75 μm column. Then, 2–28% buffer B (0.1% formic acid, 100% acetonitrile) was used to elute the peptides with a nonlinear 60 min gradient at a flow rate of 200 nl/min.

Samples were run on the Orbitrap Fusion Lumos (Thermo, USA) mass spectrometer with a Data Dependent Acquisition (DDA) method for peptide MS/MS analysis. Full scans of peptide precursors were performed from 350 to 1600 m/z at 60 K FWHM resolution with a 4×10^5 AGC target and a maximum IT of 50 ms. After a full scan, MS2 at from 100 m/z at 15 K FWHM resolution with a 5×10^4 AGC target and a maximum IT of 22 ms. HCD fragmentation was applied with 30% collision energy. The original data files were retrieved and analyzed with Proteome Discoverer 2.4 software, and the FDR was set to 0.1%. The mass spectrometry proteomics data have been deposited to the ProteomeXchange Consortium via the iProX partner repository[72, 73] with the dataset identifier PXD044715.

Statistical Analyses

The statistics were analyzed with GraphPad Prism (version 9.2.0) and R (4.2.3). The illustration is drawn with www.biorender.com. Numerical data are presented as the mean ± SEM. Statistical significance was analyzed using Student's t test for two groups and analysis of variance (ANOVA) for three or more groups. Two-way ANOVA was used to analyze differences in the learning curves of behavioral paradigms. For all analyses, $p < 0.05$ was considered statistically significant.

1. Olsen, C. and N. Wagtmann, *Identification and characterization of human DPP9, a novel homologue of dipeptidyl peptidase IV.* Gene, 2002. **299**(1-2): p. 185-93.
2. Ajami, K., et al., *Dipeptidyl peptidase 9 has two forms, a broad tissue distribution, cytoplasmic localization and DPIV-like peptidase activity.* Biochim Biophys Acta, 2004.

528 **1679**(1): p. 18-28.

529 3. Maes, M.B., et al., *Dipeptidyl peptidase 8/9-like activity in human leukocytes.* J
530 Leukoc Biol, 2007. **81**(5): p. 1252-7.

531 4. Dubois, V., et al., *Enzyme activity and immunohistochemical localization of dipeptidyl*
532 *peptidase 8 and 9 in male reproductive tissues.* J Histochem Cytochem, 2009. **57**(6):
533 p. 531-41.

534 5. Wilson, C.H., et al., *Dipeptidyl peptidase 9 substrates and their discovery: current*
535 *progress and the application of mass spectrometry-based approaches.* Biol Chem,
536 2016. **397**(9): p. 837-56.

537 6. Huang, J.C., et al., *DPP9: Comprehensive In Silico Analyses of Loss of Function*
538 *Gene Variants and Associated Gene Expression Signatures in Human Hepatocellular*
539 *Carcinoma.* Cancers (Basel), 2021. **13**(7).

540 7. Chowdhury, S., et al., *Regulation of dipeptidyl peptidase 8 and 9 expression in*
541 *activated lymphocytes and injured liver.* World J Gastroenterol, 2013. **19**(19): p. 2883-
542 93.

543 8. Schade, J., et al., *Regulation of expression and function of dipeptidyl peptidase 4*
544 *(DP4), DP8/9, and DP10 in allergic responses of the lung in rats.* J Histochem
545 Cytochem, 2008. **56**(2): p. 147-55.

546 9. Tang, Z., et al., *Contribution of upregulated dipeptidyl peptidase 9 (DPP9) in*
547 *promoting tumoregenicity, metastasis and the prediction of poor prognosis in non-*
548 *small cell lung cancer (NSCLC).* Int J Cancer, 2017. **140**(7): p. 1620-1632.

549 10. Chen, Y., et al., *Targeting dipeptidyl peptidase 8 genes inhibits proliferation, migration*

550 *and invasion by inhibition of cyclin D1 and MMP2MMP9 signal pathway in cervical*
551 *cancer.* J Gene Med, 2018. **20**(12): p. e3056.
552 11. Reinhold, D., et al., *Role of dipeptidyl peptidase IV (DP IV)-like enzymes in T*
553 *lymphocyte activation: investigations in DP IV/CD26-knockout mice.* Clin Chem Lab
554 Med, 2009. **47**(3): p. 268-74.
555 12. Finger, Y., et al., *Proteasomal degradation induced by DPP9-mediated processing*
556 *competes with mitochondrial protein import.* Embo j, 2020. **39**(19): p. e103889.
557 13. Zhang, H., et al., *Identification of novel dipeptidyl peptidase 9 substrates by two-*
558 *dimensional differential in-gel electrophoresis.* Febs j, 2015. **282**(19): p. 3737-57.
559 14. Yap, J.K.Y., et al., *The Role of Neuronal NLRP1 Inflammasome in Alzheimer's*
560 *Disease: Bringing Neurons into the Neuroinflammation Game.* Mol Neurobiol, 2019.
561 **56**(11): p. 7741-7753.
562 15. Zhong, F.L., et al., *Human DPP9 represses NLRP1 inflammasome and protects*
563 *against autoinflammatory diseases via both peptidase activity and FIIND domain*
564 *binding.* J Biol Chem, 2018. **293**(49): p. 18864-18878.
565 16. Hollingsworth, L.R., et al., *DPP9 sequesters the C terminus of NLRP1 to repress*
566 *inflammasome activation.* Nature, 2021. **592**(7856): p. 778-783.
567 17. Eichenbaum, H., *The hippocampus and declarative memory: cognitive mechanisms*
568 *and neural codes.* Behav Brain Res, 2001. **127**(1-2): p. 199-207.
569 18. Furini, C.R.G., et al., *Molecular Mechanisms in Hippocampus Involved on Object*
570 *Recognition Memory Consolidation and Reconsolidation.* Neuroscience, 2020. **435**: p.
571 112-123.

572 19. Ortega-de San Luis, C. and T.J. Ryan, *Understanding the physical basis of memory:*
573 *Molecular mechanisms of the engram.* J Biol Chem, 2022. **298**(5): p. 101866.
574 20. Neves, G., S.F. Cooke, and T.V. Bliss, *Synaptic plasticity, memory and the*
575 *hippocampus: a neural network approach to causality.* Nat Rev Neurosci, 2008. **9**(1):
576 p. 65-75.
577 21. Bear, M.F. and R.C. Malenka, *Synaptic plasticity: LTP and LTD.* Curr Opin Neurobiol,
578 1994. **4**(3): p. 389-99.
579 22. Ross, B., et al., *Structures and mechanism of dipeptidyl peptidases 8 and 9,*
580 *important players in cellular homeostasis and cancer.* Proc Natl Acad Sci U S A, 2018.
581 **115**(7): p. E1437-e1445.
582 23. Gøtzsche, C.R. and D.P. Woldbye, *The role of NPY in learning and memory.*
583 Neuropeptides, 2016. **55**: p. 79-89.
584 24. Lynch, M.A., *Long-term potentiation and memory.* Physiol Rev, 2004. **84**(1): p. 87-
585 136.
586 25. Okondo, M.C., et al., *DPP8 and DPP9 inhibition induces pro-caspase-1-dependent*
587 *monocyte and macrophage pyroptosis.* Nat Chem Biol, 2017. **13**(1): p. 46-53.
588 26. Basu, S. and R. Lamprecht, *The Role of Actin Cytoskeleton in Dendritic Spines in the*
589 *Maintenance of Long-Term Memory.* Front Mol Neurosci, 2018. **11**: p. 143.
590 27. Abbott, C.A., et al., *Cloning, expression and chromosomal localization of a novel*
591 *human dipeptidyl peptidase (DPP) IV homolog, DPP8.* Eur J Biochem, 2000. **267**(20):
592 p. 6140-50.
593 28. Bank, U., et al., *Outside or inside: role of the subcellular localization of DP4-like*

594 *enzymes for substrate conversion and inhibitor effects.* Biol Chem, 2011. **392**(3): p.
595 169-87.
596 29. Buljevic, S., et al., *The effect of CD26-deficiency on dipeptidyl peptidase 8 and 9*
597 *expression profiles in a mouse model of Crohn's disease.* J Cell Biochem, 2018.
598 **119**(8): p. 6743-6755.
599 30. Gall, M.G., et al., *Targeted inactivation of dipeptidyl peptidase 9 enzymatic activity*
600 *causes mouse neonate lethality.* PLoS One, 2013. **8**(11): p. e78378.
601 31. Kim, M., et al., *DPP9 enzyme activity controls survival of mouse migratory tongue*
602 *muscle progenitors and its absence leads to neonatal lethality due to suckling defect.*
603 Dev Biol, 2017. **431**(2): p. 297-308.
604 32. Konermann, S., et al., *Transcriptome Engineering with RNA-Targeting Type VI-D*
605 *CRISPR Effectors.* Cell, 2018. **173**(3): p. 665-676.e14.
606 33. Buchman, A.B., et al., *Programmable RNA Targeting Using CasRx in Flies.* Crispr j,
607 2020. **3**(3): p. 164-176.
608 34. Zhou, H., et al., *Glia-to-Neuron Conversion by CRISPR-CasRx Alleviates Symptoms*
609 *of Neurological Disease in Mice.* Cell, 2020. **181**(3): p. 590-603.e16.
610 35. Fanselow, M.S. and H.W. Dong, *Are the dorsal and ventral hippocampus functionally*
611 *distinct structures?* Neuron, 2010. **65**(1): p. 7-19.
612 36. Hannesson, D.K., et al., *Dorsal hippocampal kindling produces a selective and*
613 *enduring disruption of hippocampally mediated behavior.* J Neurosci, 2001. **21**(12): p.
614 4443-50.
615 37. Alves, S.H., et al., *Anxiogenic effects in the rat elevated plus-maze of 5-HT(2C)*

616 *agonists into ventral but not dorsal hippocampus.* Behav Pharmacol, 2004. **15**(1): p.
617 37-43.
618 38. Frerker, N., et al., *Neuropeptide Y (NPY) cleaving enzymes: structural and functional*
619 *homologues of dipeptidyl peptidase 4.* Peptides, 2007. **28**(2): p. 257-68.
620 39. Bjelke, J.R., et al., *Dipeptidyl peptidases 8 and 9: specificity and molecular*
621 *characterization compared with dipeptidyl peptidase IV.* Biochem J, 2006. **396**(2): p.
622 391-9.
623 40. Broqua, P., et al., *Behavioral effects of neuropeptide Y receptor agonists in the*
624 *elevated plus-maze and fear-potentiated startle procedures.* Behav Pharmacol, 1995.
625 **6**(3): p. 215-222.
626 41. Karlsson, R.M., et al., *Anxiolytic-like actions of centrally-administered neuropeptide Y,*
627 *but not galanin, in C57BL/6J mice.* Pharmacol Biochem Behav, 2005. **80**(3): p. 427-
628 36.
629 42. Corvino, V., et al., *The neurogenic effects of exogenous neuropeptide Y: early*
630 *molecular events and long-lasting effects in the hippocampus of trimethyltin-treated*
631 *rats.* PLoS One, 2014. **9**(2): p. e88294.
632 43. Huang, M., et al., *Structural and biochemical mechanisms of NLRP1 inhibition by*
633 *DPP9.* Nature, 2021. **592**(7856): p. 773-777.
634 44. Zhang, H., et al., *Advances in understanding the expression and function of dipeptidyl*
635 *peptidase 8 and 9.* Mol Cancer Res, 2013. **11**(12): p. 1487-96.
636 45. Liu, Y., et al., *Hippocampal Activation of Rac1 Regulates the Forgetting of Object*
637 *Recognition Memory.* Curr Biol, 2016. **26**(17): p. 2351-7.

638 46. Oh, D., et al., *Regulation of synaptic Rac1 activity, long-term potentiation*
639 *maintenance, and learning and memory by BCR and ABR Rac GTPase-activating*
640 *proteins.* J Neurosci, 2010. **30**(42): p. 14134-44.
641 47. Halpain, S., A. Hipolito, and L. Saffer, *Regulation of F-actin stability in dendritic*
642 *spines by glutamate receptors and calcineurin.* J Neurosci, 1998. **18**(23): p. 9835-44.
643 48. Kneussel, M. and W. Wagner, *Myosin motors at neuronal synapses: drivers of*
644 *membrane transport and actin dynamics.* Nat Rev Neurosci, 2013. **14**(4): p. 233-47.
645 49. Michaelsen, K., et al., *Fine-tuning of neuronal architecture requires two profilin*
646 *isoforms.* Proc Natl Acad Sci U S A, 2010. **107**(36): p. 15780-5.
647 50. Abouelezz, A., et al., *Tropomyosin Tpm3.1 Is Required to Maintain the Structure and*
648 *Function of the Axon Initial Segment.* iScience, 2020. **23**(5): p. 101053.
649 51. Guven, K., P. Gunning, and T. Fath, *TPM3 and TPM4 gene products segregate to the*
650 *postsynaptic region of central nervous system synapses.* Bioarchitecture, 2011. **1**(6):
651 p. 284-289.
652 52. Sheng, M. and C. Sala, *PDZ domains and the organization of supramolecular*
653 *complexes.* Annu Rev Neurosci, 2001. **24**: p. 1-29.
654 53. Luksys, G., et al., *BAIAP2 is related to emotional modulation of human memory*
655 *strength.* PLoS One, 2014. **9**(1): p. e83707.
656 54. Celestino-Soper, P.B., et al., *Use of array CGH to detect exonic copy number*
657 *variants throughout the genome in autism families detects a novel deletion in TMLHE.*
658 Hum Mol Genet, 2011. **20**(22): p. 4360-70.
659 55. Gabbott, P.L., et al., *Prefrontal cortex in the rat: projections to subcortical autonomic,*

660 *motor, and limbic centers.* J Comp Neurol, 2005. **492**(2): p. 145-77.

661 56. Bobsin, K. and H.J. Kreienkamp, *Severe learning deficits of IRSp53 mutant mice are*
662 *caused by altered NMDA receptor-dependent signal transduction.* J Neurochem,
663 2016. **136**(4): p. 752-763.

664 57. Zhou, X., et al., *Memantine Improves Cognitive Function and Alters Hippocampal and*
665 *Cortical Proteome in Triple Transgenic Mouse Model of Alzheimer's Disease.* Exp
666 Neurobiol, 2019. **28**(3): p. 390-403.

667 58. Valverde, A., et al., *Dipeptidyl peptidase 4 contributes to Alzheimer's disease-like*
668 *defects in a mouse model and is increased in sporadic Alzheimer's disease brains.* J
669 Biol Chem, 2021. **297**(2): p. 100963.

670 59. Sweeney, M.D., A.P. Sagare, and B.V. Zlokovic, *Blood-brain barrier breakdown in*
671 *Alzheimer disease and other neurodegenerative disorders.* Nat Rev Neurol, 2018.
672 **14**(3): p. 133-150.

673 60. Salminen, A., et al., *Amyloid-beta oligomers set fire to inflammasomes and induce*
674 *Alzheimer's pathology.* J Cell Mol Med, 2008. **12**(6a): p. 2255-62.

675 61. Kummer, J.A., et al., *Inflammasome components NALP 1 and 3 show distinct but*
676 *separate expression profiles in human tissues suggesting a site-specific role in the*
677 *inflammatory response.* J Histochem Cytochem, 2007. **55**(5): p. 443-52.

678 62. Izquierdo, I., et al., *Separate mechanisms for short- and long-term memory.* Behav
679 Brain Res, 1999. **103**(1): p. 1-11.

680 63. Szklarczyk, D., et al., *STRING v11: protein-protein association networks with*
681 *increased coverage, supporting functional discovery in genome-wide experimental*

682 *datasets.* Nucleic Acids Res, 2019. **47**(D1): p. D607-d613.

683 64. Shannon, P., et al., *Cytoscape: a software environment for integrated models of*
684 *biomolecular interaction networks.* Genome Res, 2003. **13**(11): p. 2498-504.

685 65. Gouveia, K. and J.L. Hurst, *Optimising reliability of mouse performance in*
686 *behavioural testing: the major role of non-aversive handling.* Sci Rep, 2017. **7**: p.
687 44999.

688 66. Yu, D.M., et al., *The in vivo expression of dipeptidyl peptidases 8 and 9.* J Histochem
689 Cytochem, 2009. **57**(11): p. 1025-40.

690 67. Leger, M., et al., *Object recognition test in mice.* Nat Protoc, 2013. **8**(12): p. 2531-7.

691 68. Wiśniewski, J.R., et al., *Universal sample preparation method for proteome analysis.*
692 Nat Methods, 2009. **6**(5): p. 359-62.

693 69. Rappsilber, J., M. Mann, and Y. Ishihama, *Protocol for micro-purification, enrichment,*
694 *pre-fractionation and storage of peptides for proteomics using StageTips.* Nat Protoc,
695 2007. **2**(8): p. 1896-906.

696 70. Demichev, V., et al., *DIA-NN: neural networks and interference correction enable*
697 *deep proteome coverage in high throughput.* Nat Methods, 2020. **17**(1): p. 41-44.

698 71. Shevchenko, A., et al., *In-gel digestion for mass spectrometric characterization of*
699 *proteins and proteomes.* Nat Protoc, 2006. **1**(6): p. 2856-60.

700 72. Ma, J., et al., *iProX: an integrated proteome resource.* Nucleic Acids Res, 2019.
701 **47**(D1): p. D1211-d1217.

702 73. Chen, T., et al., *iProX in 2021: connecting proteomics data sharing with big data.*
703 Nucleic Acids Res, 2022. **50**(D1): p. D1522-d1527.

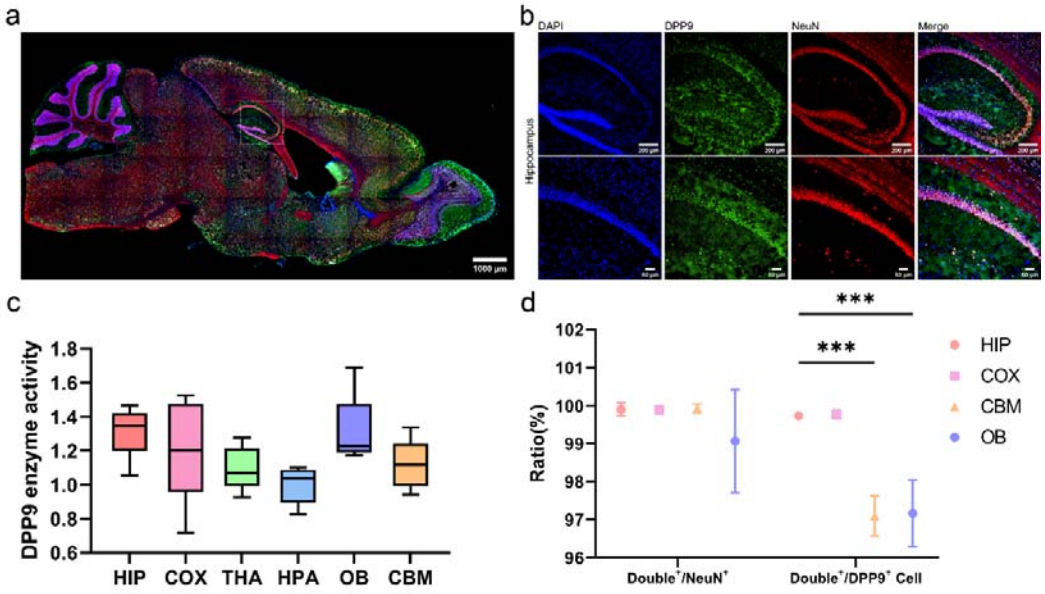

Figure 1. Distribution of DPP9 in the brain

(a) Immunofluorescence staining of mouse brain. Sagittal sections (ML: 1.00mm) DPP9 (green), NeuN (red), DAPI (blue), Scale 1000 μm. (b). Immunofluorescence staining of the mouse brain in the hippocampus. DPP9 (green), NeuN (red), DAPI (blue), 10X (upper) Scale 200 μm, 20X (downer) Scale 50 μm. (c). Enzyme activity of DPP9 in different brain regions, cortex (COX), hippocampus (HIP), thalamus (THA), hypothalamus (HPA), olfactory bulb (OB), cerebellum (CBM) (n=5, one-way ANOVA) (d). DPP9+ and NeuN+ merged cells(double +) and DPP9+ ratio in the hippocampus, cerebellum, cortex, and olfactory bulb (n=3, t test). *** $P<0.001$, Mean ± SEM.

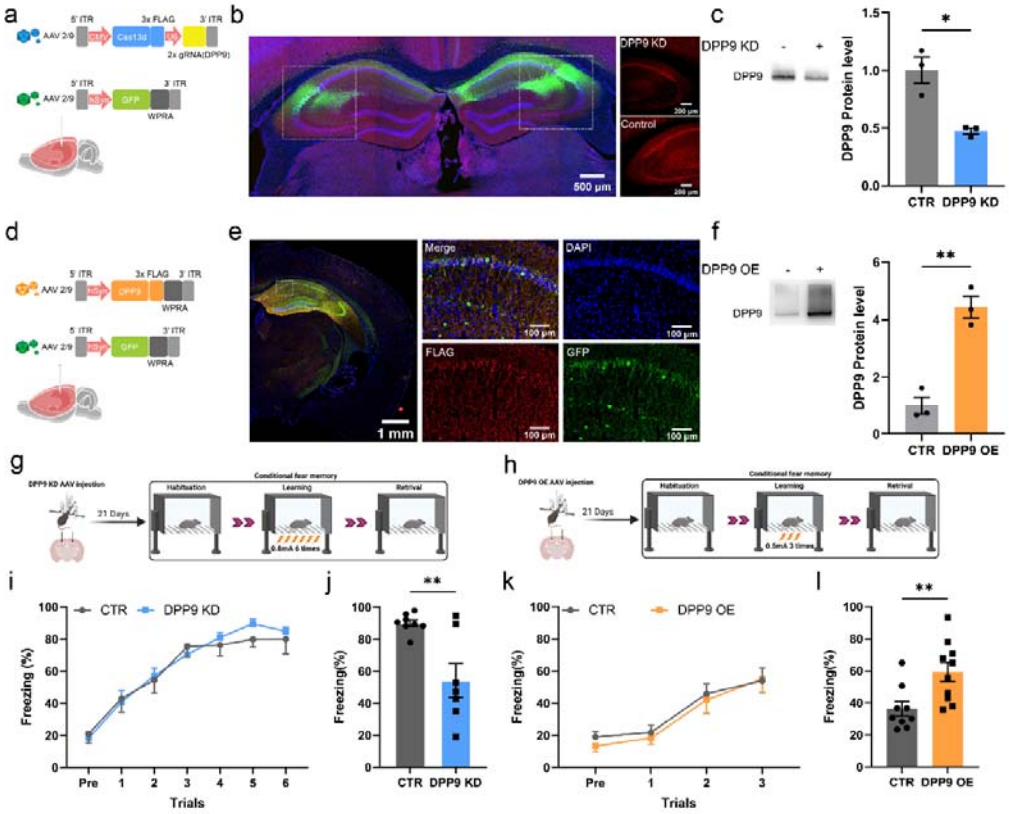

Figure 2 Model and contextual fear conditioning (CFC) on DPP9 knockdown and overexpression. a) Schematic of the AAV vector delivering Cas13d and gRNA. (b) Immunofluorescence staining of injection sites 24 h after KD AVV injection (GFP green) (DPP9 red) (DAPI blue) scale 1 mm, 100 mm. (c) Immunoblot of the hippocampus 24 h after KD AVV injection (n=3, t test). (d) Schematic of the AAV vector delivering DPP9-FLAG. (e) Immunofluorescence staining of injection sites 24 h after OE AVV injection (GFP green) (FLAG red) (DAPI blue) scale 1 mm, 100 mm. (f) Immunoblot of the hippocampus 24 h after OE AVV injection (n=3, t test). (g, h) Schematic of the CFC after KD and OE AAV injection. (i) Learning curve during CFC training (6 times, 0.8 mA) for KD mice. (n = 8, RM two-way ANOVA) (q) Learning curve during contextual fear conditioning (CFC) training (3 times, 0.5 mA) for OE mice. (n = 10, RM two-way ANOVA). (j, l) CFC

memory retrieval at day 2 in KD and CTR mice (n = 7, t test). *P<0.05, ** P<0.01, Mean ± SEM.

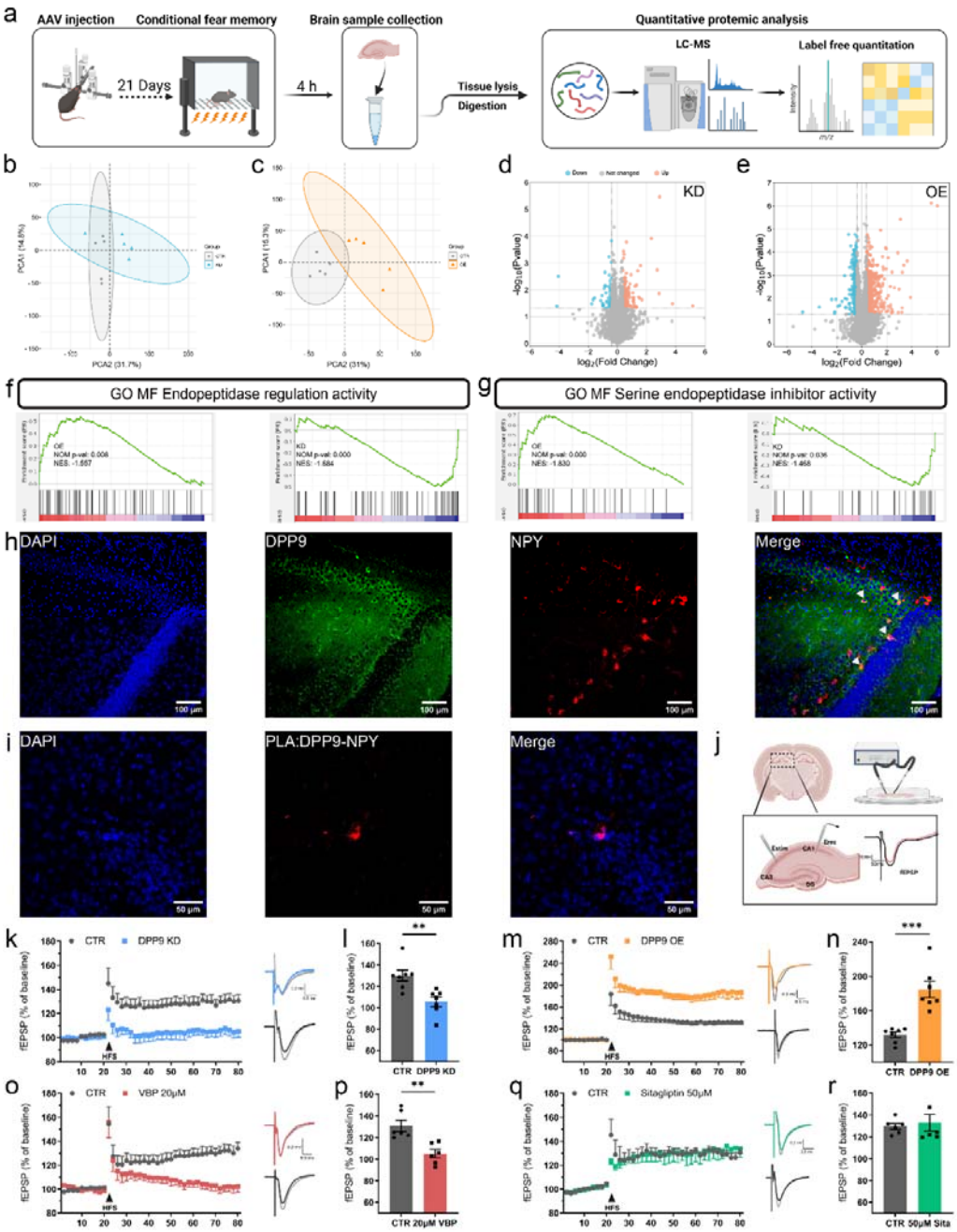

Figure 3. Proteomics of DPP9 KD and OE mice; DPP9 enzyme activity affects memory.

(a) Schematic of proteomics after CFC retrieval in KD and OE mice. (b, c) Principal component analysis (PCA) plot of all proteins from KD and OE mice. (n=5) (d, e) Volcano plots showing -Log10 P value versus fold change between KD or OE mice and CTR. (f) GSEA enhances the plot for GO:MF endopeptidase regulation activity, OE VS CTR (left), KD VS CTR (right). (g) GSEA enhances the plot for GO:MF serine endopeptidase inhibitor activity, OE vs CTR (left), KD vs CTR (right). (h) Immunofluorescence staining and colocalization of DPP9 and NPY in the hippocampus, DPP9 (green), NPY (red), DAPI (blue), Scale 100 μm. (i) Proximity ligation assay (PLA) for DPP9 and NPY in the hippocampus, PLA (red), DAPI (blue), Scale 50 μm. (j) Schematic of the recording field EPSP (fEPSP) in the hippocampus. (k-r) High-frequency stimulation (HFS, 100 Hz) induced CA1 long-term potentiation (LTP). It was maintained for at least 1 hour and lasted 20 min for the fEPSP summary. (KD, n=7, OE, n=7, Val-boroPro (VBP) 20 μM, n=6, sitagliptin 50 μM, n=6, t test) **P<0.01, *** P<0.001, mean ± SEM.

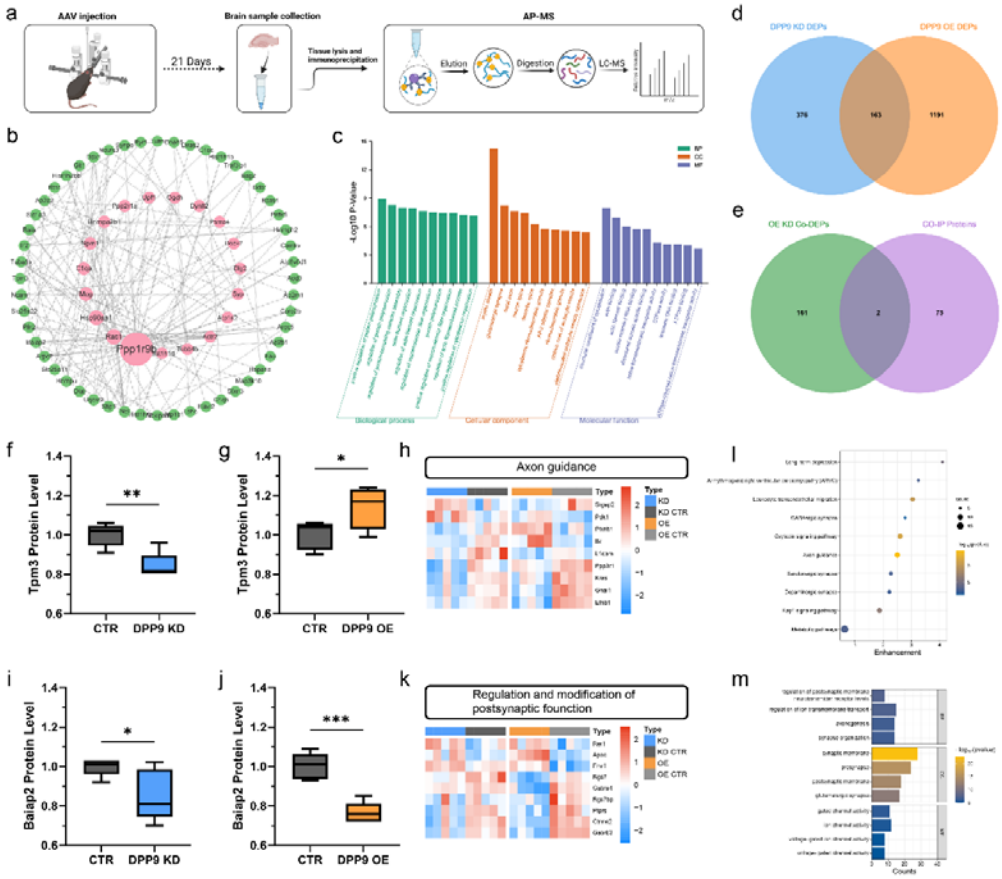

Figure 4. AP-MS of DPP9 in the hippocampus.

(a) Schematic of affinity purification and mass spectrometry (AP-MS) in mouse brain. (b) STRING PPI analysis of DPP9 interacting proteins: pink (high interactions) and green (low interactions) (n=4). (c) DPP9 interaction protein gene ontology (GO) enhancement analysis. (d) Venn diagram of DPP9 KD DEPs and DPP9 OE DEPs; there are 163 comment proteins. (e) Venn diagram of DPP9 KD-OE comment DEPs and DPP9 interaction proteins. There are 2 comment proteins (Tpm3, Baiap2). (f, g) Expression of Tpm3 in the hippocampus of DPP9 KD and OE mice (KD, n=5, OE, n=5, t test). (h) Heatmap of KD-OE comment DEPs associated with axon guidance. (I, j) Expression of Baiap2 in the hippocampus of DPP9 KD and OE mice. (KD, n=5, OE, n=5, t test) (k) Heatmap of KD-OE comment DEPs associated with regulation and modification of

postsynaptic function. (l) KEGG pathway enrichment analysis of KD-OE comment DEPs.

(j) GO enhancement analysis of KD-OE comment DEPs. *P<0.05, **P<0.01, ***P<0.001.